6th European Conference on Computational Mechanics (ECCM 6)
7th European Conference on Computational Fluid Dynamics (ECFD 7)
1115 June 2018, Glasgow, UK

SIMULATION OF PARTICLE SIZE EFFECT ON PARTICLE/MATRIX DEBONDING

TIMOTHÉE GENTIEU[1,3], ANITA CATAPANO[2], JULIEN JUMEL[1], AND JAMES BROUGHTON[3]

[1] Université de Bordeaux
I2M CNRS UMR 5295, F-33400 Talence, France
https://i2m.u-bordeaux.fr

[2] Bordeaux INP, Université de Bordeaux
I2M CNRS UMR 5295, F-33400 Talence, France
https://i2m.u-bordeaux.fr

[3] Oxford Brookes University (OBU)
Wheatley Campus, OX331HX, UK
https://www.brookes.ac.uk/tde/

Key words: Particle reinforced material, Debonding, CZM, LEFM, size effect

Abstract. The present study aims to describe the debonding phenomenon of a single particle embedded in an elastic matrix. A numerical simulation based on a Cohesive Zone Model (CZM) is employed to simulate the particle debonding from the matrix. This model relies on two mechanical parameters: the strength of the interface σ_{max} and the interface fracture energy G_c. The results show that bigger particles tend to debond before smaller ones. This particle size effect on debonding is captured by the CZM. Moreover, for big particles, the debonding seems to be governed by the strength of the interface, whereas, for small ones, the predominant quantity is the fracture energy.

1 INTRODUCTION

The addition of stiff particles in a matrix is a common practice to obtain a reinforced material stiffer and more resistant than the bulk matrix itself. Such a resulting composite material is used in multiple industries such as automotive, aeronautics, aerospace, etc. Various mechanical properties can be obtained using different materials, sizes, shapes, geometries, or surface treatments for the reinforcements. The role of the particles is then preponderant in such a material behaviour. That is the reason why it is important to be able to correctly estimate their influence either in the elastic domain or when damage occurs.

Three main damage mechanisms are commonly observed in particle reinforced materials: particle failure, microcracks nucleating in the matrix and particle debonding from

the matrix [1]. For a polymer reinforced with rigid particles, debonding is the first damage mechanism to be activated and is considered to be the main toughening mechanism [2]. A clear particle size effect has been observed experimentally [3]. Indeed, the global toughness of the material increases with particle size [4].

To deal with this particle size effect, an energy balance has often been evoked in the literature. In the context of Linear Elastic Fracture Mechanics (LEFM), several authors develop an expression of the stress responsible for particle debonding [2], [5], [6], [7], [8]. All those studies are based on the same assumptions: a rigid spherical particle of a radius R is embedded in an infinite matrix, which elastic properties are E_m (Young's modulus) and ν_m (Poisson's ratio). The interface is supposed to be infinitely stiff and its fracture energy is denoted G_c. When a hydrostatic loading is remotely applied to the matrix, the critical interface stress is then:

$$\sigma_c = \sqrt{\frac{G_c}{R}\frac{4E_m}{1+\nu_m}}. \tag{1}$$

According to this energy-based relationship, the critical stress to debond a particle is proportional to $1/\sqrt{R}$.

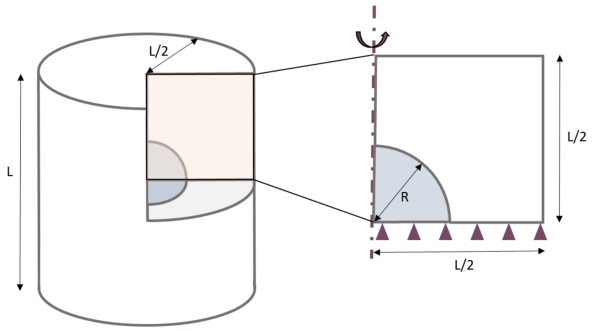

Figure 1: Spherical particle embedded in a cylindrical matrix; geometric reduction of the problem using axial symmetries.

The case study for the spherical particle debonding consists in one single particle embedded in a cylinder of matrix. The geometry of the Representative Volume Element (RVE) is the one presented in Fig. 1. The radius of the sphere is equal to one tenth of the length of the diameter of the cylinder: $R = L/10$. This situation corresponds to a dilute particle volume fraction $\phi = 0.0042$. The geometry is reduced to a 2D structure by axisymmetry, and then only half of the geometry is modelled by using a mirror symmetry along the horizontal axis.The material properties associated to the particle are those of the boron-carbide while the matrix is an epoxy resin. The mechanical properties of the particle, the matrix and the interface are detailed in Table 1. Moreover the following hypothesis always apply to the present study:

1. the material behaviour of both particles and matrix is linear elastic;

2. the interface is supposed to be infinitely stiff.

	$E\ [GPa]$	$\nu\ [\ ]$	$\sigma_{max}\ [MPa]$	$G_c\ [J.m^{-2}]$
Particle	450	0.2	×	×
Matrix	3	0.3	×	×
Interface	∞	×	50	100

Table 1: Mechanical properties of the materials and the interface

In the Finite Elements (FE) framework, the problem of a crack propagating at an interface between two surfaces is commonly treated with Cohesive Zone Models (CZM), where cohesive interactions at the interface are able to describe the progressive nonlinear failure behaviour. In Section 2, the CZM applied to spherical particle debonding will be described. Then, in Sections 3 and 4, the debonding of this particle will be respectively studied under hydrostatic and uniaxial tensile loadings. Finally, a discussion on these results will be held.

2 THE COHESIVE ZONE MODEL (CZM) APPLIED TO SPHERICAL PARTICLE DEBONDING

In order to numerically solve the debonding problem, a FE analysis is carried out. Zero-thickness elements are introduced at the interface and their behaviour is described by a CZM. The CZM is a traction-separation law linking the stress and the relative displacement at the interface between two surfaces. Multiple traction-separation law shapes have been developed such as bilinear, trilinear, exponential, etc. In the present study, only the bilinear law will be employed (see Fig. 2) which corresponds to the CZM of [9] in the software Ansys. The bilinear law is defined by two main parameters: the strength of the interface σ_{max} and the fracture energy G_c. σ_{max} corresponds to the peak of the traction-separation law, whereas G_c corresponds to the shaded area under the curve. As we consider the interface to be perfect until failure, the slope of the first part of the traction-separation law is taken high enough so that the global stiffness of the RVE is not affected by this additional compliance. The introduction of the two parameters σ_{max} and G_c in the traction-separation law induces the apparition of a critical displacement u_c which, according to Leguillon [10], is not a material parameter but a structural one. We can deduce the critical displacement u_c as a function of σ_{max} and G_c as follows:

$$u_c = \frac{2G_c}{\sigma_{max}} \tag{2}$$

During the first part of the loading, the interface deforms elastically. After the strength value σ_{max} is reached, the interface starts to get damaged. Indeed, its stiffness is progressively degraded until the relative displacement of the two surfaces reaches the value u_c where the stiffness of the interface completely vanishes. The two surfaces are then considered to be completely debonded.

According to the case study described on Fig. 1, the RVE consists in a quarter of a disk embedded in a square of matrix (see Fig. 3). A specific care has been given the generation of the mesh. In particular, the mesh has been refined at the interface to ensure

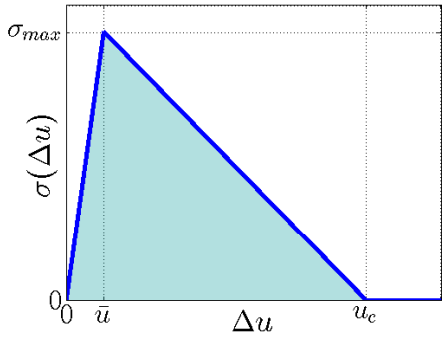

Figure 2: Bilinear traction-separation law

both a good convergence and a good precision for the results around the zone of interest. On the other hand, the rest of the RVEis discretised with larger element sizes to reduce computational costs. The arc representing the matrix/particle interface is discretised into 180 elements, therefore each cohesive element correspond to an opening angle of 0.5°. The following boundary conditions are applied to ensure mirror symmetries of the RVE:

$$\begin{cases} U_x(x=0)=0, \\ U_y(y=0)=0. \end{cases} \tag{3}$$

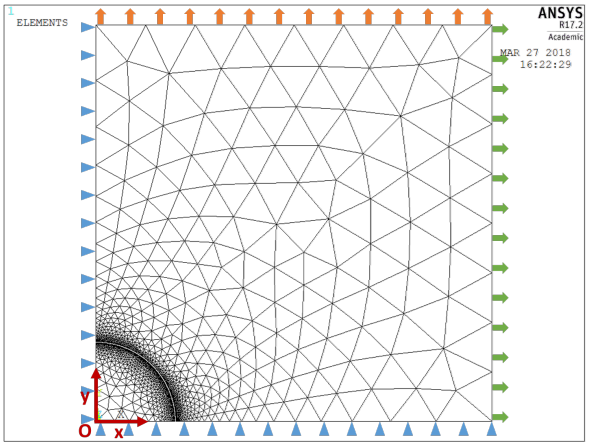

Figure 3: Geometry, mesh and loading conditions of the RVE.

For each loading condition studied in this article, the geometry and the mesh of the RVE are replicated in a homothetic manner and the CZM is used to determine the remote stress responsible for the onset of the particle debonding from the matrix. The remote stress and the strain are calculated as:

$$\begin{cases} \sigma = \left(\sum\limits_{\text{nodes}} F_i \right) / \left(\pi L^2 \right), \\ \epsilon = U/L, \end{cases} \tag{4}$$

where n_i is the i-th node submitted to the imposed displacement U and F_i is the corresponding reaction force.

3 DEBONDING OF A SINGLE SPHERICAL PARTICLE UNDER HYDROSTATIC LOADING

The debonding of the spherical particle under hydrostatic loading is here analysed. A displacement U is imposed at the boundaries of the RVE in order to get a hydrostatic stress state (see Fig. 3, the imposed displacement corresponds to the green and orange arrows):

$$\begin{cases} U_x(x = L) = U, \\ U_y(y = L) = U. \end{cases} \tag{5}$$

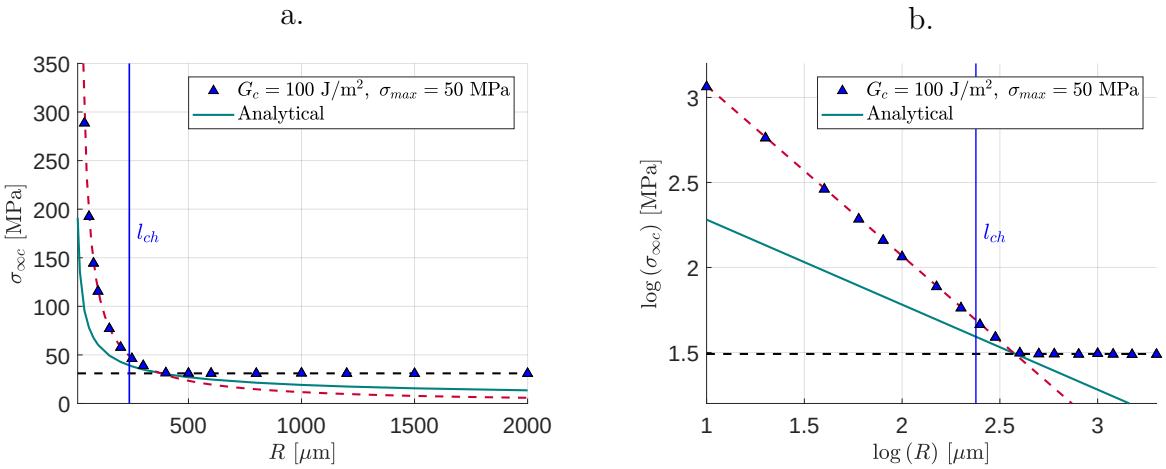

Figure 4: a. Critical remote stress against particle radius for hydrostatic loading (the dots correspond to the CZM results and the dashed lines to asymptotes); b. Same plot in log-log scale.

The critical stress responsible for the debonding onset is determined for multiple particle sizes (with radii varying between $10\mu m$ and $2mm$) using both the CZM approach and the analytical one represented in Eq. 1. The results are represented on Fig. 4 a. We can observe that for small particles ($R \leq 400\mu m$), the critical stress increases with decreasing particle size. For larger particles ($R \geq 400\mu m$), a plateau value is reached and the critical stress remains constant. A characteristic length l_{ch} has been defined by several authors to establish the ductile to brittle transition in fracture mechanics. A definition of l_{ch}, taking into account the stiffness heterogeneity of the composite and based on [11], is chosen in this article:

$$l_{ch} = \frac{G_c E_{eff}}{{\sigma_{max}}^2}, \tag{6}$$

with E_{eff} the effective Young's modulus of the bi-material, calculated as the harmonic mean of the particle and matrix Young's moduli E_p and E_m:

$$E_{eff} = \left(\left(E_p^{-1} + E_m^{-1}\right)/2\right)^{-1}. \tag{7}$$

This characteristic length is represented on Fig. 4 a., and one can observe that it represents fairly well the transition between the radius-dependent to radius-independent regimes.

To assess more precisely the radius dependency of the critical remote stress, the same graph is plotted in a log-log scale on Fig. 4 b. In bothe Fig. 4 a. and b. the asymptotes are plotted with dashed lines. It can be observed that for small particles, the slope of the CZM asymptote is equal to -1, whereas the slope of the analytical expression is $-1/2$. $\sigma_{\infty c}$ is then proportional to $1/R$ with the CZM and $1/\sqrt{R}$ for the analytical expression. For large particles, characterised by $R > l_{ch}$, $\sigma_{\infty c}$ is independent of the particle radius. It is noteworthy that the stress concentration at the interface is also independent of particle radius [12], whereas the energy release rate isn't [13]. This observation suggests that for large particles, the strength of the interface becomes the predominant factor for the interface failure.

4 DEBONDING OF A SINGLE SPHERICAL PARTICLE UNDER UNIAXIAL LOADING

In this section, the debonding of the spherical particle under uniaxial loading is studied. A displacement U is imposed at the upper boundary ($y = L$) of the RVE only in order to get a uniaxial stress state (the imposed displacement corresponds to the orange arrows represented on Fig. 3). The right boundary ($x = L$) is left free so that the loading conditions can be summed up as:

$$U_y(y = L) = U. \tag{8}$$

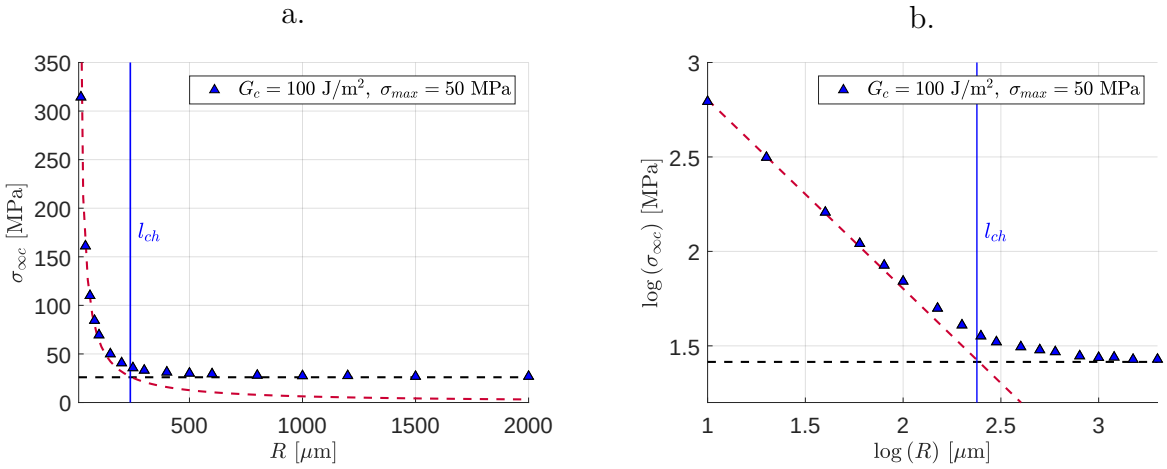

Figure 5: a. Critical remote stress against particle radius with CZM under uniaxial loading; b. Same plot in log-log scale.

The remote stress responsible for the debonding onset is depicted on Fig. 5 a. The same behaviour as the one observed for the hydrostatic loading is described here: below a given particle size, the smaller the particle gets the higher the critical stress, while for larger particles, $\sigma_{\infty c}$ remains constant. The same graph is plotted on Fig. 5 b. in

a log-log scale. On both Fig. 5 a. and 5 b. asymptotes are drawn with dashed lines. The intersection of the asymptotes for the two regimes is exactly located at l_{ch} calculated using Eq. 6. However, contrary to the hydrostatic loading, an intermediate behaviour is observed between the radius-dependent and radius-independent regions of the graph. In this regime, the CZM induces an important effect of the extension of the damaged region in the crack nucleation process. This length depends on the traction-separation law shape and consequently on both interface strength and fracture energy.

5 DISCUSSION

To assess the influence of the different physical quantities involved in fracture (fracture energy G_c, strength of the interface σ_{max}, critical displacement u_c, characteristic length l_{ch}), a parametric study is conducted. Four CZM are employed and their properties are expressed in Table 2.

	$G_c\ [J.m^{-2}]$	$\sigma_{max}\ [MPa]$	$u_c\ [mm]$	$l_{ch}\ [mm]$
CZM 1	100	50	0.004	238.4
CZM 2	50	50	0.002	119.2
CZM 3	200	100	0.004	119.2
CZM 4	100	100	0.002	59.6

Table 2: CZM properties

The CZM 1 and 2 share the same strengths σ_{max}. The CZM 1 and 3 share the same critical displacements u_c. The CZM 1 and 4 share the same critical energies G_c. The results for the critical remote stress against the particle radius are plotted on Fig. 6 a. for the 4 different CZM. Fig. 6 b. represents the same plot in a log-log scale.

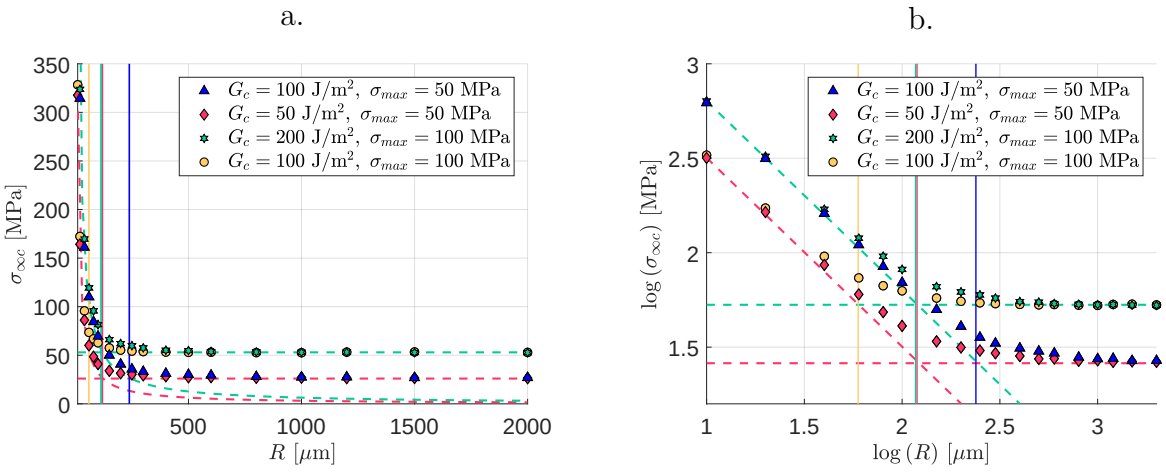

Figure 6: a. Critical remote stress against particle radius for different CZM; b. Same plot in log-log scale.

As previously observed, two asymptotic regimes are observed for small and large particles. The characteristic length l_{ch} seems to be a very good descriptor of the transition between the two regimes as it corresponds to the intersection of the asymptotes for all the CZM. For small particles, the critical remote stresses obtained using the CZM 1 and 3 are the same. This result seems to imply that the predominant CZM parameter for small particle debonding is the critical length u_c. For large particles, the plateau values of $\sigma_{\infty c}$ when using CZM 1 and 2 are the same. This last result confirms that the strength σ_{max} of the CZM governs the debonding for large particle sizes. A final remark concerns the results related to the CZM 1 and 4 which share the same fracture energy: the respective remote stresses don't have any asymptote in common. The authors do not identified the main reason of this phenomenon and a research work is still in progress.

6 CONCLUSIONS

In this work the debonding phenomenon of a spherical particle embedded in a matrix has been analysed. In particular the particle size effect on the critical remote stress has been evaluated. Two different loading cases have been considered: hydrostatic and the uniaxial tensile loading. The same conclusions can be drawn concerning the particle size effect on the debonding phenomenon:

- larger particles tend to debond at lower remote stress states than smaller particles;
- for large particles, the critical remote stress is constant. The predominant debonding parameter is the strength of the interface, as the stress state at the interface is independent of the particle radius;
- for small particles, the critical remote stress increases when decreasing the particle size. When using the CZM, this critical remote stress is proportional to $1/R$, whereas when using the analytical expression based on an energy balance, the critical remote stress is proportional to $1/\sqrt{R}$. A similar result was observed for fibre-reinforced composites in [11]. The debonding of small particles simulated by a CZM seems to be governed by the critical displacement.

The characteristic length l_{ch} seems to be a fairly accurate value of the transition from the radius-dependent regime to the radius-independent one. For the uniaxial loading, the value of l_{ch} is exactly at the intersection between the two asymptotes. For the hydrostatic loading, l_{ch} only gives a good order of magnitude of the radius at the transition zone. For the hydrostatic loading, the numerical results are exactly equal to the asymptotic ones. For the uniaxial loading, the asymptotic behaviours are observed only when $R \ll l_{ch}$ and $R \gg l_{ch}$ respectively. For this last case, an intermediate behaviour is described around l_{ch} by the CZM. In order to establish this particle size effect, a comparison between these results obtained with a CZM are compared to the ones obtained with the Finite Fracture Mechanics (FFM) in an article in process [14]. In the framework of FFM, a crack of a finite length opens and propagates when both an energy and a stress criteria are simultaneously fulfilled. The FFM is able to analytically catch the evolution of the debonding stress with particle radius.

ACKNOWLEDGEMENTS

DGA of France, supporting the first author through *Allocation de thèse 2015*, is gratefully acknowledged.

REFERENCES

[1] JK Chen and M Yuan. Decoupling of viscous dissipation and damage dissipation in particulate-reinforced polymeric materials. *Computational materials science*, 40(2):267–274, 2007.

[2] JK Chen, ZP Huang, and J Zhu. Size effect of particles on the damage dissipation in nanocomposites. *Composites Science and Technology*, 67(14):2990–2996, 2007.

[3] S Fu, X Feng, B Lauke, and Y Mai. Effects of particle size, particle/matrix interface adhesion and particle loading on mechanical properties of particulate–polymer composites. *Composites Part B: Engineering*, 39(6):933–961, 2008.

[4] Y Nakamura, M Yamaguchi, M Okubo, and T Matsumoto. Effect of particle size on the fracture toughness of epoxy resin filled with spherical silica. *Polymer*, 33(16):3415–3426, 1992.

[5] B Lauke. Effect of particle size distribution on debonding energy and crack resistance of polymer composites. *Computational Materials Science*, 77:53–60, 2013.

[6] JG Williams. Particle toughening of polymers by plastic void growth. *Composites science and technology*, 70(6):885–891, 2010.

[7] M Zappalorto, M Salviato, and M Quaresimin. Assessment of debonding-induced toughening in nanocomposites. *Procedia Engineering*, 10:2973–2978, 2011.

[8] M Salviato, M Zappalorto, and M Quaresimin. Nanoparticle debonding strength: A comprehensive study on interfacial effects. *International Journal of Solids and Structures*, 50(20):3225–3232, 2013.

[9] G Alfano and MA Crisfield. Finite element interface models for the delamination analysis of laminated composites: mechanical and computational issues. *International journal for numerical methods in engineering*, 50(7):1701–1736, 2001.

[10] D Leguillon. Strength or toughness? a criterion for crack onset at a notch. *European Journal of Mechanics-A/Solids*, 21(1):61–72, 2002.

[11] IG García, Marco Paggi, and V Mantič. Fiber-size effects on the onset of fiber–matrix debonding under transverse tension: A comparison between cohesive zone and finite fracture mechanics models. *Engineering Fracture Mechanics*, 115:96–110, 2014.

[12] JN Goodier. Concentration of stress around spherical and cylindrical inclusions and flaws. *J. appl. Mech*, 1(1):39–44, 1933.

[13] J Cho, MS Joshi, and CT Sun. Effect of inclusion size on mechanical properties of polymeric composites with micro and nano particles. *Composites Science and Technology*, 66(13):1941–1952, 2006.

[14] T Gentieu, A Catapano, J Jumel, and J Broughton. Size effect in particle debonding: Comparisons between finite fracture mechanics and the cohesive zone model. *In progress*, 2018.